Riemannian space tessellation with polyhedral room images

Jean-Dominique Polack, Aidan Meacham, Roland Badeau, Jean-Christophe Valière

▶ **To cite this version:**

Jean-Dominique Polack, Aidan Meacham, Roland Badeau, Jean-Christophe Valière. Riemannian space tessellation with polyhedral room images. 16ème Congrès Français d'Acoustique, CFA2022, Société Française d'Acoustique; Laboratoire de Mécanique et d'Acoustique, Apr 2022, Marseille, France. hal-03848222

HAL Id: hal-03848222
https://hal.science/hal-03848222v1

Submitted on 10 Nov 2022

HAL is a multi-disciplinary open access archive for the deposit and dissemination of scientific research documents, whether they are published or not. The documents may come from teaching and research institutions in France or abroad, or from public or private research centers.

L'archive ouverte pluridisciplinaire **HAL**, est destinée au dépôt et à la diffusion de documents scientifiques de niveau recherche, publiés ou non, émanant des établissements d'enseignement et de recherche français ou étrangers, des laboratoires publics ou privés.

16ème Congrès Français d'Acoustique
11-15 Avril 2022, Marseille

Riemannian space tessellation with polyhedral room images

J-D. Polack [a], A. Meacham [a], R. Badeau [b] J-C. Valière [c]

[a] Sorbonne Univ., CNRS, Institut ∂'Alembert UMR 7109, Paris, France

[b] Télécom Paris, Institut Polytechnique de Paris, LTCI, Palaiseau, France

[c] Univ. Poitiers, CNRS, PPRIME UPR3346, Poitiers, France

Counting the image sources of rectangular rooms is a well known technique, based on mirroring the original rooms on all its walls in order to tesselate the Euclidian space, leading to a quadratic increase with layer order. We show that a similar mirroring technique can be applied to polygonal and polyhedral rooms of arbitrary shapes, leading to the tessellation of a Riemannian space with negative curvature. From this tessellation we derive a close formulation for counting the numbers of image sources, which increases exponentially with layer order. Thus, a bridge between rooms with flat walls and generic mixing rooms with partially curved walls is obtained.

1 Introduction

Computing the number of image sources for a rectangular enclosure is an easy task that acousticians routinely carry out [1]. Indeed, as all the images of the room tesselate the Euclidean space, the computation simply amounts to dividing the volume of a sphere of radius ct, where c is the speed of sound and t the time elapsed since the source emited, by the volume of the original room, as each image room, or cell, only contains one image source. Thus one obtains a number of image sources that increases with the square of the time elapsed since the source emitted and is inversely proportional to the volume of the room, and most acousticians consider that this approximation is also valid for rooms of arbitrary shapes.

Few authors have questionned the validity of this approximation for rooms of arbitrary shapes. [3] has argued that this number should increase exponentially for mixing rooms, as a consequence of the conservation of the phase space measure. Indeed, in mixing rooms, any small volume of the phase space, for example the initial volume around the source, exponentially expands in at least one phase dimension as it propagates with time, and exponentially decreases in at least one dimension, so that any volume decays into exponentially thin stripes. Any elementary cell of the phase space thus intersects exponentially many stripes, corresponding to exponentially many image sources.

Polyhedral rooms, on the other hand, are not mixing rooms since two neighbouring rays in the phase space almost certainly separate linearly with time, and not exponentially. Thus, the preceding argument cannot be used to evaluate the number of image sources. The present paper therefore addresses the non trivial issue of computing the number of images sources for arbitrary polyhedral enclosures.

2 Images of obtuse angles

We first consider the obtuse angle β of Fig. 1 in a 2-dimensional Euclidean space. A sound source S (black star) emitting inside the angle emits rays in all directions. Some rays impinge on the left arm Ox of the angle and are reflected (red arrows). As the position of impact moves clockwise toward the apex, the reflected ray gradually moves upwards and eventually hits the right arm on which it is reflected once more. Finally, the ray impacts the apex of the angle (black upwards broken-line arrow).

In a similar fashion, some rays will impinge on the right arm Oy and be reflected (green arrows). As the position of impact moves anticlockwise toward the apex, the reflected ray gradually moves upwards and eventually hits the left arm on which it is reflected once more. Despite the continuity of the impinging rays around the apex, there is no continuity of the reflected rays, and this creates scattering.

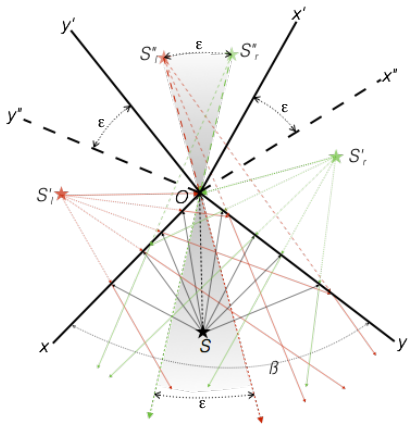

FIGURE 1 – Reflection and scattering of sound rays on obtuse angle β. ε is the excess angle, since second order image angles overlap by ε.

In order to visualise the scattering, one needs to consider the images of the sources by reflection on the two arms of the angle. Let's call S'_l the image of the source on the left arm (red star), and S'_r the image on the right arm (green star) ; S''_l the left-most second order image (dim red star), and S''_r the right-most second order image (dim green star). Reflected rays on the arms of the angle are first emitted from the first order image sources S'_l and S'_r, then from the second order sources S''_l and S''_r when the reflected rays hit the opposite arm, until the rays emitted from the first-order image sources reach the apex (red and green dotted-line arrows). In that position, the rays emitted from the second order image sources do not coincide in direction, since they are emitted from two different image sources at angle ε with respect to the apex. Scattering therefore comes in to *fill the gap* between these two directions, and in fact beyond them. In other words, one must consider a continuum of image sources along the sector between S''_l and S''_r (grey sector), that is, one must rotate the second order image angle by ε from position $y''0x'$ to position $y'0x''$.

In fact, when rays rotate *clockwise* around the original source S, the reflected rays rotate *anticlockwise* around the first order source S''_l, and *clockwise* around the second order source S''_r. So, when the secondary source moves *clockwise* from S''_l to S''_r on Fig. 1, the diffracted rays rotate *clockwise* around the apex, thus filling the grey sector with continuity of rotations at its boundaries.

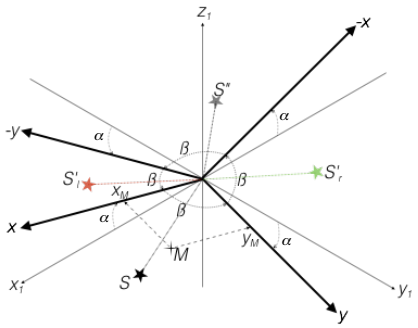

FIGURE 2 – Embedding scattering on obtuse angle in 3-dimensional space. Angles α are vertical and measure deviations of angle arms from horizontal plane. Note that the two second order image sources coalesce in one single image source.

In order to make the second order image angles coincide, one needs to embed Fig. 1 in a 3-dimensional space as in Fig. 2. We call x_1, y_1, and z_1 the three Cartesian coordinates, and keep notations Ox and Oy for the arms of the original flat angular sector, which is now slanted so that angle β exactly projects on a right angle. As a consequence, Ox is elevated by angle α above Ox_1 and Oy is lowered by angle α below Oy_1 ; similarly, $O(-x)$ is elevated by angle α above $O(-x_1)$ and $O(-y)$ is lowered by angle α below $O(-y_1)$, so that the apex angle remains equal to β. In such a way, we obtain a *locally flat* space where rays are free to cross the borders between subsequent angular sectors without changing their direction. But computation of the local metric tensor [4] shows that the spaces has negative curvature at the apex O where it tends toward $4(\frac{\pi}{2}-\beta)$ for small values of $\frac{\pi}{2}-\beta$. Indeed, Regge [5] has shown that the curvature is equal to the total deficit angle at the apex $-\varepsilon = 2\pi - 4\beta$.

For a 3-dimensional obtuse dihedral angle, Fig 1 represents a projection of the rays on a plane perpendicular to the apical edge. But no equivalent of Fig 2 can be drawn, as the embedding takes place in a 4-dimensional space. Full computation shows that the local curvature remains null everywhere - flat space - except on the apical edge. In the limit where β tends toward a right angle, the curvature around the apical edge is equal to $(2\pi - 4\beta)\ell$, where ℓ is the length of the apical edge, called *hinge* by [5]. Note that hinges are subspaces of co-dimension 2 where excess angle is non null.

3 Number of image sources

Let us now consider polygonal (2-dimensional case) or polyhedral rooms (3-dimensional case). We impose the restriction, that will be discussed at the end of this Section, that all the internal angles of the polygons are right or obtuse in order to obtain the 4 sectors of Figs. 1 and 2. In the polyhedral case, beside keeping all internal dihedral angles right or obtuse for the same reason, we also impose that all vertices are shared by three faces only. Typical examples are pentagons in 2-dimensions, and dodecahedra in 3-dimensions.

3.1 Convex polygonal rooms

For convex polygonal rooms with n edges, the n first order images are obtained by reflection on the edges. However, the order of reflection is not relevant for counting the images : layers are much more relevant. Thus, on Fig. 3, the numbers correspond to the successive layers around the original room.

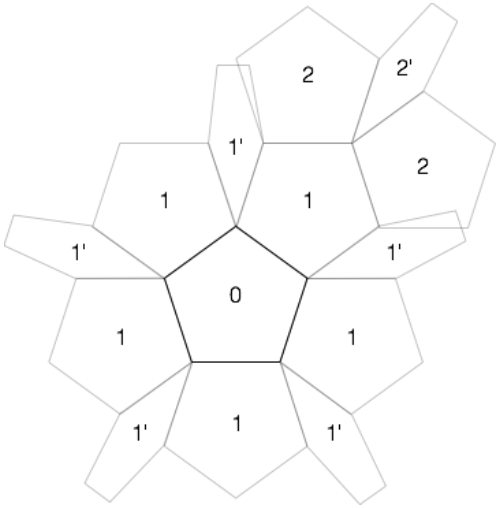

FIGURE 3 – Image rooms of pentagon. Primed images are skewed in order to fit in the picture. Numbers correspond to successive layers of images, with 0 denoting the original room and primes one supplementary order of reflection (see text). Note that one supplementary image must be added each time image rooms overlap (e.g. between 1′and 2).

Accordingly, the first layer is composed of the n images on the edges, to which n supplementary images, one at each vertex, are added. For the next layers, it is more efficient to compute separately the number of free edges and the number of free vertices, that is, edges and vertices that are not common to two adjacent images : one adds one image for each free edge, and one for each free vertex, exactly as for the first layer. It can be seen on Fig. 3 that edge images create $(n-3)$ free edges and $(n-4)$ free vertices ; and vertex images crate $(n-2)$ free edges and $(n-3)$ free vertices. Note that $n \geqslant 4$ if all angles are right or obtuse. Let's call e_i the number of free edges and v_i the number of free vertices of layer i. One obtains the recurrence formula :

$$\begin{pmatrix} e_i \\ v_i \end{pmatrix} = \begin{pmatrix} n-3 & n-2 \\ n-4 & n-3 \end{pmatrix} \begin{pmatrix} e_{i-1} \\ v_{i-1} \end{pmatrix} = \Lambda^i \begin{pmatrix} e_0 \\ v_0 \end{pmatrix} \quad (1)$$

where $\Lambda = \begin{pmatrix} n-3 & n-2 \\ n-4 & n-3 \end{pmatrix}$ and $\det \Lambda = 1$. The eigenvalues of matrix Λ are respectively $\lambda_1 = \frac{1}{2}(\sqrt{n-2} + \sqrt{n-4})^2 \geqslant 1$ and $\lambda_2 = \frac{1}{2}(\sqrt{n-2} - \sqrt{n-4})^2 \leqslant 1$.

Case $n = 4$: If $n = 4$, we obtain rectangular rooms, for which the number of image sources increases linearly with the layer order. Indeed, in this case, the matrix is upper triangular :

$$\Lambda = \begin{pmatrix} 1 & 2 \\ 0 & 1 \end{pmatrix} \tag{2}$$

with $\lambda_1 = \lambda_2 = 1$, and the computation of eq. (1) is straightforward :

$$\Lambda^i = \begin{pmatrix} 1 & 2i \\ 0 & 1 \end{pmatrix} \tag{3}$$

As expected, we obtain for rectangular rooms $e_i = 4(2i + 1)$ and $v_i = 4$: the number of corners remains constant and equal to 4, with a linear increase of the number of edge images. And the total number of image sources $\mathfrak{N}_i$ of layer i is $\mathfrak{N}_i = e_i + v_i = 8(i + 1)$, that is, increases linearly with i.

Case $n > 4$: If $n \geqslant 5$, then $\lambda_1 > 1$ and $\lambda_2 < 1$, and the eigenvectors are given by :

$$X_1 = \begin{pmatrix} \sqrt{n-2} \\ \sqrt{n-4} \end{pmatrix},\ X_2 = \begin{pmatrix} \sqrt{n-2} \\ -\sqrt{n-4} \end{pmatrix} \tag{4}$$

and the total number of image sources $\mathfrak{N}_i$ of layer i is given by the sum of the two contributions, that is :

$$\begin{aligned} \mathfrak{N}_i &= e_i + v_i \\ &\approx \frac{n(\sqrt{n-2} + \sqrt{n-4})^{2i+1}}{2^{i+1}} \left(\frac{1}{\sqrt{n-4}} + \frac{1}{\sqrt{n-2}} \right) \\ &= \frac{n(\sqrt{n-2} + \sqrt{n-4})^{2(i+1)}}{2^{i+1}\sqrt{(n-2)(n-4)}} \end{aligned} \tag{5}$$

Example : For a **pentagon**, $n = 5$ and the eigenvalues are $\lambda_1 = \frac{1}{2}(\sqrt{3} + 1)^2 \approx 3.73$ and $\lambda_2 = \frac{1}{2}(\sqrt{3} - 1)^2 \approx 0.27$. Matrix Λ is now equal to :

$$\Lambda = \begin{pmatrix} 2 & 3 \\ 1 & 2 \end{pmatrix} \tag{6}$$

and the total number of image sources $\mathfrak{N}_i$ of layer i is given by eq. (5) :

$$\mathfrak{N}_i = e_i + v_i \approx \frac{5\left(\sqrt{3} + 1\right)^{2(i+1)}}{2^{i+1}\sqrt{3}} \tag{7}$$

In other words, the number of image sources increases exponentially with the order of the layer, a very different behaviour than for rectangular rooms, but similar to mixing rooms [3].

3.2 Convex polyhedral rooms

For convex polyhedral rooms, it is not sufficient to only consider the number N of faces. We must also consider the number n_i of edges of each face i. We thus obtain :

- the number of faces : $F = \sum_i 1 = N$
- the number of edges : since one edge is common to 2 faces, this number is $E = \frac{1}{2}\sum_i n_i$
- the number of vertices : with the assumption that vertices are shared by 3 faces only, this number is $V = \frac{1}{3}\sum_i n_i$

With the help of Euler's polyhedron formula $F - E + V = 2$, valid for convex polyhedra, we obtain :

$$F - E + V = \sum_i \left[1 - \frac{n_i}{2} + \frac{n_i}{3}\right] = \sum_i \left[1 - \frac{n_i}{6}\right] = 2 \tag{8}$$

that is, introducing the mean number of edges per face $\bar{n} = \frac{1}{N}\sum_i n_i$:

$$(6 - \bar{n})N = 12 \tag{9}$$

As a consequence, the mean number of edges per face, the total number of edges, and the total number of vertices are given by :

$$\bar{n} = \frac{6(N-2)}{N},\ E = 3(N-2),\ V = 2(N-2) \tag{10}$$

As in Sect. 3.1, we consider successive layers of image rooms built around the original rooms, and we compute separately the number of free faces, edges and vertices belonging to the images created by free faces, edges an vertices. If we call f_m, e_m and v_m the numbers of free faces, edges and vertices respectively in layer m, we obtain the recurrence formulae :

$$\begin{pmatrix} f_{m+1} \\ e_{m+1} \\ v_{m+1} \end{pmatrix} = \Lambda \begin{pmatrix} f_m \\ e_m \\ v_m \end{pmatrix} = \Lambda^{m+1} \begin{pmatrix} f_0 \\ e_0 \\ v_0 \end{pmatrix} \tag{11}$$

with matrix Λ given by :

$$\Lambda = \begin{pmatrix} N - \bar{n} - 1 & N - 4 & N - 3 \\ \left(\frac{N}{2} + 1\right)\bar{n} - \bar{n}^2 & \left(\frac{N}{2} - 4\right)\bar{n} + 5 & \left(\frac{N}{2} - 3\right)\bar{n} + 3 \\ \left(\frac{N}{3} + 2\right)\bar{n} - \bar{n}^2 & \left(\frac{N}{3} - 4\right)\bar{n} + 8 & \left(\frac{N}{3} - 3\right)\bar{n} + 5 \end{pmatrix} \tag{12}$$

and its determinant equal to :

$$-\lambda^3 + \lambda^2\left[\frac{6(N-4)^2}{N} - 1\right] - \lambda\left[\frac{6(N-4)^2}{N} - 1\right] + 1 = 0 \tag{13}$$

Case $N = 6$: If $N = 6$, we obtain rectangular parallelepiped rooms, for which eq. (10) reduces to $n_i = \bar{n} = 4$ for all i, $e_0 = 12$, and $v_0 = 8$ with $f_0 = N = 6$. In this case, the matrix is upper triangular :

$$\Lambda = \begin{pmatrix} 1 & 2 & 3 \\ 0 & 1 & 3 \\ 0 & 0 & 1 \end{pmatrix} \tag{14}$$

Since all diagonal terms are equal to 1, the three eigenvalues are equal to 1 and the computation of eq. (11) is straightforward :

$$\Lambda^i = \begin{pmatrix} 1 & 2i & 3i^2 \\ 0 & 1 & 3i \\ 0 & 0 & 1 \end{pmatrix} \tag{15}$$

We obtain for rectangular parallelepiped rooms $f_i = 6(2i + 1)^2$, $e_i = 12(2i + 1)$ and $v_i = 8$: as expected,

the number of corners remains constant and equal to 8, with a linear increase of the number of edge images and a quadratic increase of the number of the face images. And the total number of image sources $\mathfrak{N}_i$ of layer i is $\mathfrak{N}_i = f_i + e_i + v_i = 24(i+1)^2 + 2$, that is, increases quadratically with i.

Case $N > 6$: The direct solution of eq. (13) gives then the three eigenvalues :

- $\lambda_0 = 1$,
- $\lambda_1 = \left[\frac{3(N-4)^2}{N} - 1\right] + \frac{N-4}{N}\sqrt{3[(N-6)(3N-8)]} > 1$,
- $\lambda_2 = \left[\frac{3(N-4)^2}{N} - 1\right] - \frac{N-4}{N}\sqrt{3[(N-6)(3N-8)]} < 1$.

with eigenvectors :

$$X_0 = \begin{pmatrix} (N-3) \\ 0 \\ -\frac{(N-2)(N-6)}{N} \end{pmatrix},\ X_1 = \begin{pmatrix} \sqrt{3[(N-6)(3N-8)]} \\ +\frac{3(N-6)(3N-8)}{N} \\ \frac{2(N-6)\sqrt{3[(N-6)(3N-8)]}}{N} \end{pmatrix},$$
$$X_2 = \begin{pmatrix} \sqrt{3[(N-6)(3N-8)]} \\ -\frac{3(N-6)(3N-8)}{N} \\ \frac{2(N-6)\sqrt{3[(N-6)(3N-8)]}}{N} \end{pmatrix} \tag{16}$$

For large values of the layer number i, $\lambda_2^i \longrightarrow 0$, and eq. (11) is approximated by :

$$\begin{pmatrix} f_i \\ e_i \\ v_i \end{pmatrix} \approx \frac{\left[\sqrt{\frac{3}{N}}(N-4) + \sqrt{\frac{(N-6)(3N-8)}{N}}\right]^{2i}}{2^{i+1}(3N-8)} \begin{pmatrix} N-2 & \frac{N\sqrt{3[(N-6)(3N-8)]}}{3(N-6)} \\ \frac{(N-2)\sqrt{3[(N-6)(3N-8)]}}{N} & 3N-8 \\ \frac{3(N-2)(N-6)}{N} & 2\sqrt{3[(N-6)(3N-8)]} \\ \frac{N(N-3)\sqrt{3[(N-6)(3N-8)]}}{3(N-6)} & (N-3)(3N-8) \\ & 2(N-3)\sqrt{3[(N-6)(3N-8)]} \end{pmatrix} \begin{pmatrix} f_0 \\ e_0 \\ v_0 \end{pmatrix} \tag{17}$$

and $\mathfrak{N}_i = f_i + e_i + v_i$

Example : For a **dodecahedron**, $N = 12$ with $\bar{n} = 5$, $e_0 = 30$, and $v_0 = 20$ with $f_0 = N = 12$. The eigenvalues are $\lambda_0 = 1$, $\lambda_1 = 15+4\sqrt{14} \approx 29.97$ and $\lambda_2 = 15-4\sqrt{14} = 0.03$. Matrix Λ is now equal to :

$$\Lambda = \begin{pmatrix} 9 & 8 & 9 \\ 10 & 15 & 18 \\ 5 & 8 & 10 \end{pmatrix} \tag{18}$$

and the total number of image sources $\mathfrak{N}_i$ of layer i is given by the sum of the 3 terms in eq. (17), that is :

$$\begin{aligned} \mathfrak{N}_i &= f_i + e_i + v_i \\ &\approx \frac{\left(15+4\sqrt{14}\right)^i}{46}\left(5\left[4+\sqrt{14}\right]f_0 + 2\left[15+2\sqrt{14}\right]e_0\right. \\ &\left. + 37\left[7+4\sqrt{14}\right]v_0\right) = \frac{10(29.97)^i\left(316+157\sqrt{14}\right)}{23} \end{aligned} \tag{19}$$

In other words, the number of image sources increases exponentially with the order of the layer, as is the case for polygonal rooms with more than 4 edges.

4 Conclusion

We have presented a geometrical theory that naturally accounts for scattering on the boundaries of a room. It introduces Riemannian spaces with negative curvature, which constitute the proper setting for the distribution of images created by non-rectangular rooms with obtuse angles, that is, created by irregular polyhedra. The crucial factor is the excess angle that arises around specific edges, called hinges, when first and second order images are considered, as it pilots the curvature of the space.

From this Riemannian tessellation, we have proposed a scheme for counting the number of image sources. Here, the parameter is not the order of reflection, but counting the layers of images around the original room. Only free faces, edges and vertices are taken into account to build the layers, and it makes it possible to give a closed-form formula for the number of image sources in case all dihedral angles are obtuse : the number of images increases exponentially, making polyhedral rooms similar to mixing rooms in this respect. We did not explicitly solved for the cases when some dihedral angles are reflex or acute, but gave some indications as how to handle them.

Références

[1] L. Cremer and H. A. Müller. *Die wissenschaftlichen Grundlagen der Raumakustik*, volume Band I, page 25. Hirzel Verlag, Stuttgart (1978).

[2] G. Naylor Ed. Special issue on computer modelling and auralisation of sound fields in rooms. *Applied Acoustics*, **38**(2-4) (1993).

[3] J.D. Polack. Modifying chambers to play billiards : the foundations of reverberation theory. *Acustica*, **76**, 257-272 (1992).

[4] J.D. Polack, A. Meacham, R. Badeau and J.C. Valière. Riemannian space tessellation with polyhedral room images. hal-03598258 (2022).

[5] T. Regge. General Relativity without Coordinates. *Il Nuovo Cimento*, **XIX**, 558-571, (Feb. 1961).